Journal of Rock Mechanics and Geotechnical Engineering 9 (2017) 671–682

Contents lists available at ScienceDirect

Journal of Rock Mechanics and Geotechnical Engineering

journal homepage: www.rockgeotech.org

Full Length Article

Nonlinear shear behavior of rock joints using a linearized implementation of the Barton–Bandis model

Simon Heru Prassetyo [a,*], Marte Gutierrez [a], Nick Barton [b]

[a] Department of Civil and Environmental Engineering, Colorado School of Mines, Golden, CO 80401, USA
[b] Nick Barton and Associates, Oslo, Norway

ARTICLE INFO

Article history:
Received 1 October 2016
Received in revised form
28 December 2016
Accepted 4 January 2017
Available online 10 July 2017

Keywords:
Rock joints
Joint shear behavior
Friction and dilation
Barton–Bandis (B–B) model
Equivalent Mohr–Coulomb (M–C) parameters

ABSTRACT

Experiments on rock joint behaviors have shown that joint surface roughness is mobilized under shearing, inducing dilation and resulting in nonlinear joint shear strength and shear stress vs. shear displacement behaviors. The Barton–Bandis (B–B) joint model provides the most realistic prediction for the nonlinear shear behavior of rock joints. The B–B model accounts for asperity roughness and strength through the joint roughness coefficient (*JRC*) and joint wall compressive strength (*JCS*) parameters. Nevertheless, many computer codes for rock engineering analysis still use the constant shear strength parameters from the linear Mohr–Coulomb (M–C) model, which is only appropriate for smooth and non-dilatant joints. This limitation prevents fractured rock models from capturing the nonlinearity of joint shear behavior. To bridge the B–B and the M–C models, this paper aims to provide a linearized implementation of the B–B model using a tangential technique to obtain the equivalent M–C parameters that can satisfy the nonlinear shear behavior of rock joints. These equivalent parameters, namely the equivalent peak cohesion, friction angle, and dilation angle, are then converted into their mobilized forms to account for the mobilization and degradation of *JRC* under shearing. The conversion is done by expressing *JRC* in the equivalent peak parameters as functions of joint shear displacement using proposed hyperbolic and logarithmic functions at the pre- and post-peak regions of shear displacement, respectively. Likewise, the pre- and post-peak joint shear stiffnesses are derived so that a complete shear stress-shear displacement relationship can be established. Verifications of the linearized implementation of the B–B model show that the shear stress-shear displacement curves, the dilation behavior, and the shear strength envelopes of rock joints are consistent with available experimental and numerical results.
© 2017 Institute of Rock and Soil Mechanics, Chinese Academy of Sciences. Production and hosting by Elsevier B.V. This is an open access article under the CC BY-NC-ND license (http://creativecommons.org/licenses/by-nc-nd/4.0/).

1. Introduction

Rock masses contain various types of discontinuities, such as bedding planes, joints, shear zones, and faults, which distinguish them from other materials. Joints are commonly observed and widespread in rocks. Unless they are healed and mineralized, joints have weakening effects on the strength of rock masses because they do not have tensile resistance and their shear strength is usually much smaller compared to the intact rock matrix (Priest, 1993; Singhal and Gupta, 2010). In a fractured rock mass, the shear behavior of rock joints is particularly important because it dominantly controls the deformability, strength, and hence the stability of the rock mass. For example, the conditions for slip on major pervasive features in fractured rock masses, such as block sliding from a slope or block falling in an underground excavation, are controlled not only by the shear strength of the particular joint but also by its dilation along asperities under shearing (Goodman, 1976, 1989; Barton and Hansteen, 1979; Barton, 1982). This dilation is caused by the mobilization of joint surface roughness, and it will cause nonlinearity in the shear strength as well as strain hardening and strain softening in the shear behavior of rock joints. Therefore, it is essential for fractured rock models to take into account this nonlinearity so that the realistic response of fractured rock masses can be accurately predicted, leading to the economical and reliable design and analysis of excavations and structures in rocks.

Extensive laboratory experiments on rock joint behavior from the early 1960s to date have shown that the shear behavior of rock

* Corresponding author.
E-mail address: sprasset@mymail.mines.edu (S.H. Prassetyo).
Peer review under responsibility of Institute of Rock and Soil Mechanics, Chinese Academy of Sciences.

http://dx.doi.org/10.1016/j.jrmge.2017.01.006
1674-7755 © 2017 Institute of Rock and Soil Mechanics, Chinese Academy of Sciences. Production and hosting by Elsevier B.V. This is an open access article under the CC BY-NC-ND license (http://creativecommons.org/licenses/by-nc-nd/4.0/).

joints is nonlinear. This nonlinearity is significantly affected by the dilation-induced joint roughness, causing the nonlinear relationship between joint shear stress τ and normal stress σ_n (e.g. Barton, 1973, 1982, 2016; Barton and Choubey, 1977; Bandis et al., 1981; Barton et al., 1985; Indraratna and Haque, 2000; Hencher and Richards, 2015). Surprisingly, and as pointed out by Barton (2016), the joint roughness and wall strength parameters, known as the contributing parameters to the nonlinearity of the shear strength of rock joints, were initially ignored and rejected by leading researchers in reservoir geomechanics, following development of the parameters in rock mechanics in the 1970s. The widespread use of linear behavior assumptions could lead to errors in reservoir interpretation since joint roughness-induced behaviors such as dilation, aperture increase, permeability increase as well as nonlinear closure reversing the above were effectively ignored.

Patton (1966) was one of the first to consider the effect of joint roughness on the nonlinear shear behavior of rock joints by conducting a series of direct shear tests on saw-tooth triangular joints. He proposed a bilinear shear strength criterion consisting of two linear segments intersecting a normal stress called the transition stress. The shear strength of a joint is governed by the sliding along the joint asperities when the normal stress is less than the transition stress and by the partial shearing through asperities when the normal stress is above the transition stress. Ladanyi and Archambault (1969) improved Patton's model by developing a shear strength criterion that considers simultaneous sliding and shearing of rock joints instead of separating the two mechanisms. However, the model is still challenging to be implemented due to the difficulty in obtaining the transition stress and the inclination angle parameters for irregular joint surfaces. Goodman (1976) was the first to develop a rock joint model in the general framework of the finite element method, which later stimulated researchers in rock mechanics to enhance the application of joint models in numerical modeling. Unfortunately, Goodman's model did not consider the effect of surface roughness degradation under shearing.

The Barton–Bandis (B–B) joint model is currently the most realistic empirical model for predicting shear failure behavior of rough joints (Barton, 1973; Barton and Choubey, 1977; Bandis, 1980; Barton et al., 1985). In the B–B model, the peak shear strength of a rock joint is determined by the following criterion:

$$\tau = \sigma_n \tan\left[JRC \log_{10}\left(\frac{JCS}{\sigma_n}\right) + \phi_r\right] \tag{1}$$

where *JRC* is the joint roughness coefficient, *JCS* is the joint wall compressive strength, and ϕ_r is the joint residual friction angle.

The main advantages of the B–B model are: (1) it has been established based on and extensively verified against a wide range of experimental results; (2) the parameters involved have real physical meanings; and (3) the parameters can be easily determined using simple index tests. The B–B model takes into account the increase in shear strength due to the mobilization of surface roughness or strain hardening during pre-peak shearing and its reduction or strain softening due to asperity degradation during post-peak shearing (Barton, 1982). By considering the pre- and post-peak behaviors, shear stress-shear displacement curves can be formulated for a wide range of input data, using Barton's dimensionless mobilized *JRC* concept (see Fig. 1, dotted line). This is an important part of the B–B model.

Due to its simplicity, rock mechanics engineers are still accustomed to use the linear Mohr–Coulomb (M–C) failure criterion for modeling fractured rock mass behavior (Bhasin and Barton, 1997), particularly in the continuum modeling approach. In addition, due to the historical development of rock mechanics, many stability analyses of excavations in jointed rock masses still use strength parameters in terms of cohesion and friction angle from the M–C failure criterion. The M–C criterion relates the shear stress τ and the normal stress σ_n at failure as

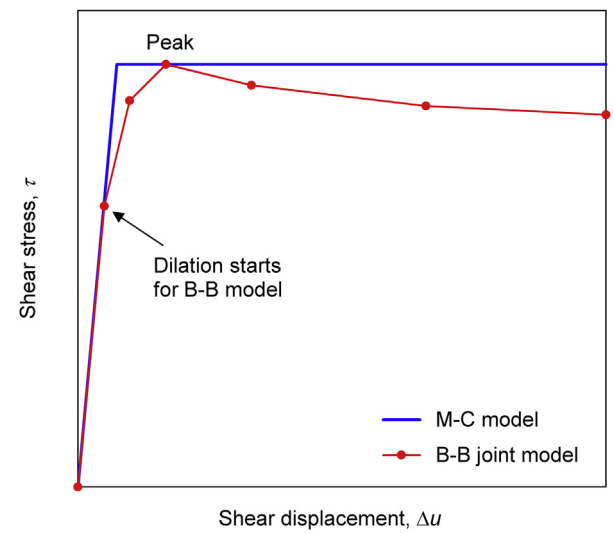

Fig. 1. Illustration of a shear stress vs. shear displacement curve from the mobilized *JRC* concept based on specific input data. It is compared with the closest (bilinear) Mohr–Coulomb (M–C) model.

$$\tau = c + \sigma_n \tan\phi \tag{2}$$

where c is the cohesion, and ϕ is the friction angle. Needless to say, the M–C criterion is linear in the τ vs. σ_n axes, gives constant cohesion and friction angle, and does not consider the mobilization and reduction of joint surface roughness. Therefore, unlike in the B–B model, the strain hardening and strain softening behaviors of rock joints are not captured in the linear and perfectly-plastic M–C model (Fig. 1, solid line).

The shear strength criterion in the B–B model (Eq. (1)) is nonlinear and plots as a curved failure surface in the τ vs. σ_n axes. Fig. 2 shows plots of the B–B failure criterion as functions of different values of *JRC* and for typical values of $JCS = 50$ MPa and $\phi_r = 30°$. With increasing *JRC* and σ_n, the B–B criterion becomes

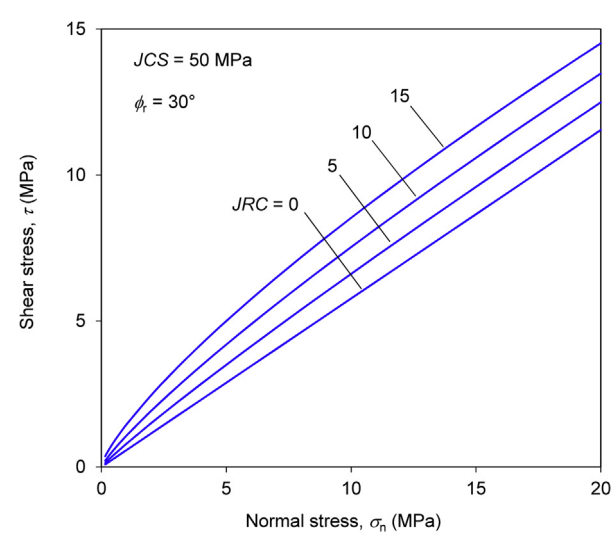

Fig. 2. The B–B failure criterion for different *JRC* values at $JCS = 50$ MPa and $\phi_r = 30°$.

more curved and nonlinear. For $JRC = 0$, the B–B criterion corresponds to the M–C criterion with $\phi = \phi_r$ (cohesion is assumed zero). It should be noted that as the normal stress climbs towards the value of *JCS*, increased confined strength is assumed. The diameter of the relevant Mohr circle (σ_1–σ_3) should replace *JCS* according to recommendations given by Barton (1976).

Nevertheless, despite the capability of the B–B model to characterize the nonlinear shear behavior of rock joints, many legacy computer codes for rock engineering analysis, such as Abaqus (Simulia, 2012), fast Lagrangian analysis of continua (FLAC) (Itasca, 2011) and Plaxis (Plaxis bv, 2016), still use the linear M–C model. Thus, given the need for realistic joint modeling, it will be beneficial if the B–B model can be implemented in these computer codes by directly linking the existing linear M–C joint models with the nonlinear B–B model. This link can be achieved by obtaining the *equivalent* M–C parameters by "multi-linearization" of the B–B values. In addition, the equivalent mobilized shear strength parameters can also be obtained to account for joint roughness mobilization and reduction as a function of shear displacement as was done by Barton (1982). In this way, the benefit of the simplicity of the linear M–C model in legacy computer codes can be coupled with the advanced but quite simple-to-understand capabilities of the nonlinear B–B model.

2. Methods of linearization

There are two approaches to obtain mathematically equivalent *linear* M–C parameters from the *nonlinear* B–B failure criterion, namely: (1) the equivalent tangent friction angle ϕ_t and cohesion c_t given, respectively, by the slope and intercept of the tangent to the nonlinear failure surface at the current (effective) normal stress, and (2) the equivalent *secant* friction angle ϕ_t and zero cohesion, given by drawing an intersecting line from the origin to the current (effective) normal stress at the failure surface. The two concepts to obtain the linear failure parameters are illustrated in Fig. 3. As can be seen, due to the nonlinearity in the shear failure behavior of rock joint, the friction angles in both approaches are not constant but vary with normal stress. In the equivalent tangent approach, nonzero cohesion is obtained, which is purely an apparent cohesion value that results from the linearization. As commonly known, joints do not have cohesive strength, unless the joints have extremely steep steps, as where a secondary joint set is crossed by the previously formed and continuous primary joint set.

As an example of the secant linearization concept, Fig. 4 shows the variation of the equivalent secant friction angle ϕ_s from the B–B model for different *JRC* values at $JCS = 50$ MPa and $\phi_r = 30°$. As indicated, ϕ_s is not constant but decreases with the increase in normal stress due to the nonlinearity of the relationship between shear strength and normal stress. It can also be seen that within the range of $\sigma_n < JCS$, the equivalent secant friction angle ϕ_s is larger than $\phi_r = 30°$ for $JRC > 0$, again due to the additional friction provided by the dilation along the asperities.

3. Linearization of the B–B model

The B–B model is linearized using a similar approach to the tangential technique shown in Fig. 3 to obtain the equivalent *peak* M–C parameters that can satisfy the nonlinear shear behavior of rock joints. These equivalent peak parameters, namely the equivalent peak cohesion, friction angle, and dilation angle, are then converted into their mobilized forms to account for the mobilization (during hardening) and degradation (during softening) of *JRC* under shearing. The full tangential linearization of the B–B model involves two steps: (1) deriving the equivalent peak parameters from the B–B shear failure criterion, and (2) relating these equivalent linear parameters to Barton (1982)'s mobilized roughness and shear displacement relations in the hardening and softening regimes.

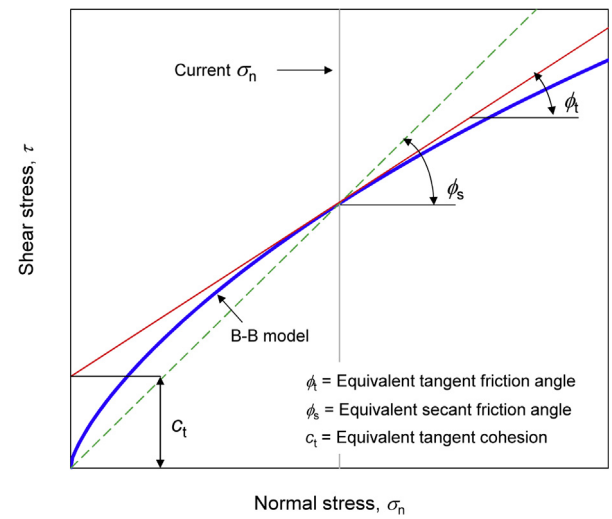

Fig. 3. Illustration of the equivalent tangent friction angle ϕ_t and cohesion c_t and equivalent secant friction angle ϕ_s at the current stress σ_n from the nonlinear B–B model.

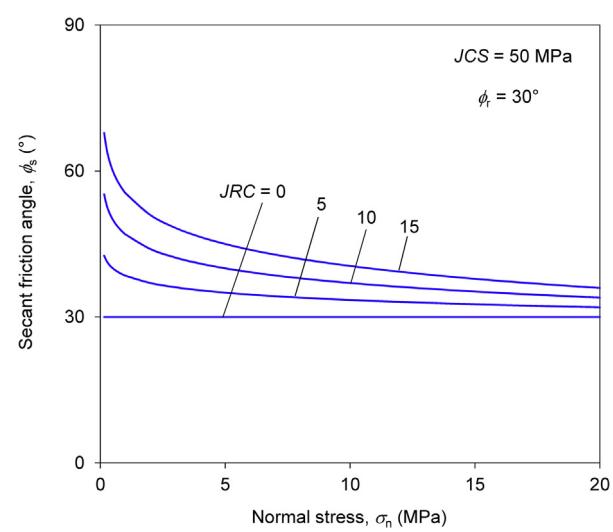

Fig. 4. Equivalent linear secant friction angle ϕ_s from the nonlinear B–B model for different *JRC* values at $JCS = 50$ MPa and $\phi_r = 30°$.

3.1. Deriving the equivalent peak parameters c_t, ϕ_t and ψ_t

The equivalent peak parameters can be derived by relating c and ϕ from the conventional M–C model to *JRC*, *JCS* and ϕ_r from the B–B model. In the literature, these equivalent parameters may have appeared in different forms and have been called instantaneous strength parameters (Deb, 2012; Liu et al., 2014). Adopting the same shear strength as in the B–B model, the equivalent peak shear strength in the equivalent M–C model can be expressed as

$$\tau_t = c_t + \sigma_n \tan \phi_t \tag{3}$$

where c_t is the equivalent peak cohesion, and ϕ_t is the equivalent peak friction angle expressed as

$$\phi_t = JRC \log_{10}\left(\frac{JCS}{\sigma_n}\right) + \phi_r \tag{4}$$

Using Eqs. (3) and (4), the inclination of the tangent to the nonlinear failure surface at the current normal stress σ_n in the B–B model is expressed as

$$\tan\phi_t = \frac{d\tau}{d\sigma_n} = \frac{d}{d\sigma_n}\left\{\sigma_n \tan\left[JRC \log_{10}\left(\frac{JCS}{\sigma_n}\right) + \phi_r\right]\right\} \tag{5}$$

By using the product rule:

$$(fg)' = f'g + fg' \tag{6}$$

and by setting

$$f = \sigma_n, \quad g = \tan\left[JRC \log_{10}\left(\frac{JCS}{\sigma_n}\right) + \phi_r\right] \tag{7}$$

the first term on the right hand side of Eq. (6) becomes

$$f'g = \tan\left[JRC \log_{10}\left(\frac{JCS}{\sigma_n}\right) + \phi_r\right] = A \tag{8}$$

To obtain fg', the following chain rule can be used:

$$\frac{du}{dx} = \frac{du}{dv}\frac{dv}{dx} \tag{9}$$

By setting

$$u = \tan v, \quad v = JRC \log_{10}\left(\frac{JCS}{\sigma_n}\right) + \phi_r, \quad x = \sigma_n \tag{10}$$

the terms on the right hand side of Eq. (9) can be expanded as

$$\frac{du}{dv} = 1 + \tan^2 v = 1 + \tan^2\left[JRC \log_{10}\left(\frac{JCS}{\sigma_n}\right) + \phi_r\right] = 1 + A^2 \tag{11}$$

$$\frac{dv}{dx} = -\frac{JRC}{\sigma_n \ln 10} \tag{12}$$

Using Eqs. (9)–(12), the second term on the right hand side of Eq. (6) can be expressed as

$$fg' = -\left(1 + A^2\right)\frac{JRC}{\ln 10} = -B \tag{13}$$

Note that all quantities are in radians. Finally, by using Eqs. (8) and (13), Eq. (5) becomes

$$\tan\phi_t = \tan\left[JRC \log_{10}\left(\frac{JCS}{\sigma_n}\right) + \phi_r\right] - \left(1 + A^2\right)\frac{JRC}{\ln 10} = A - B \tag{14}$$

and hence the equivalent peak friction angle becomes

$$\phi_t = \arctan(A - B) \tag{15}$$

The equivalent peak cohesion c_t can be found by equating Eqs. (1) and (2) with the use of Eq. (14) as

$$c_t = \sigma_n B \tag{16}$$

According to Maksimovic (1996), the essential components of the shear strength of rock joints consist of cohesion c, friction angle ϕ, and dilation angle ψ. Using this principle, Eq. (3) can be rewritten as

$$\tau_t = c_t + \sigma_n \tan(\phi_r + \psi_t) \tag{17}$$

and hence the equivalent peak dilation angle ψ_t is simply given by

$$\psi_t = \phi_t - \phi_r \tag{18}$$

The next step is to relate the equivalent peak parameters derived above to the joint roughness–shear displacement relationships during hardening and softening and convert the peak parameters from the *constant* forms to the *mobilized* forms.

3.2. Relating the equivalent peak parameters to joint roughness-shear displacement relation

To relate c_t, ϕ_t and ψ_t to the joint roughness coefficient JRC vs. shear displacement Δu relations, two analytical curve fitting functions are proposed to smooth out the discrete and piecewise-linear paired values of JRC_m/JRC_p vs. $\Delta u/\Delta u_p$ developed by Barton (1982) as shown in Fig. 5. The parameters JRC_p and Δu_p correspond to the peak values of JRC and Δu at the peak shear strength, respectively. Meanwhile, the parameter JRC_m corresponds to the mobilized values of JRC that vary according to the level of Δu relative to its peak value Δu_p.

For the shear displacement in the pre-peak strain hardening region, $\Delta u \le \Delta u_p$, a hyperbolic function is proposed to capture the mobilization of joint roughness up to JRC_p. The function is expressed as

$$\frac{JRC_m}{JRC_p} = \frac{a\,(\Delta u/\Delta u_p)}{1 + b\,(\Delta u/\Delta u_p)} \tag{19}$$

where a and b are the constants to be determined to fit the discrete values given by Barton (1982). For the shear displacement in the post-peak strain softening region, $\Delta u > \Delta u_p$, a logarithmic function is proposed to capture the reduction of the roughness until it approximately reaches the residual value ($JRC = 0$). The function is expressed as

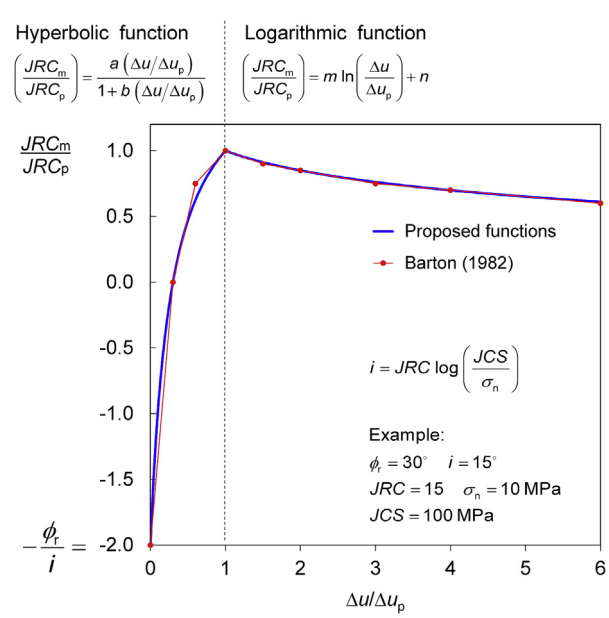

Fig. 5. Concept of joint roughness mobilization (Barton, 1982).

$$\frac{JRC_m}{JRC_p} = m \ \ln\left(\frac{\Delta u}{\Delta u_p}\right) + n \tag{20}$$

where m and n are also the constants to be determined from the discrete values.

3.2.1. The pre-peak hyperbolic function

Two non-zero sets of data points are required: one at the start of dilation at $\Delta u/\Delta u_p = 0.3$, and the other at the peak displacement at $\Delta u/\Delta u_p = 1$. For the sake of derivation, all data points on the y-axis in Fig. 5 will be increased by ϕ_r/i, where i represents the effect of irregular asperities on the fracture surface and is defined as $i = JRC \ \log_{10}(JCS/\sigma_n)$, so that JRC_m/JRC_p will start from zero. Eq. (19) can be rewritten as

$$y' = \frac{ax'}{1 + bx'} \tag{21}$$

where $y' = JRC_m/JRC_p$ and $x' = \Delta u/\Delta u_p$. Examining Eq. (21) at $x' = 0.3$ and $x' = 1$ gives the expression for y' as shown in Eqs. (22) and (23), respectively, as

$$\frac{\phi_r}{i}\ (1 + 0.3b) = 0.3a \tag{22}$$

$$\left(1 + \frac{\phi_r}{i}\right)\ (1 + b) = a \tag{23}$$

Multiplying Eq. (23) by 0.3 and subtracting the resulting equation from Eq. (22), the constant b can be solved as

$$b = \frac{7}{3}\ \frac{\phi_r}{i} - 1 \tag{24}$$

The constant a can then be obtained from Eq. (22) as

$$a = \frac{10}{3}\ \frac{\phi_r}{i}\ (1 + 0.3b) \tag{25}$$

By substituting the values of a and b back into Eq. (19), the *apparent* JRC_m will be obtained. The *true* JRC_m in the pre-peak strain hardening region is then given by subtracting $(\phi_r/i)\ JRC_p$ from the *apparent* JRC_m which gives

$$JRC_{m_pre} = \left[\frac{7(1 + \phi_r/i)\ \Delta u/\Delta u_p}{3 - (3 - 7\phi_r/i)\ \Delta u/\Delta u_p} - 1\right]\ \frac{\phi_r}{i}\ JRC_p \tag{26}$$

3.2.2. The post-peak logarithmic function

To develop the logarithmic function in the post-peak region, the standard curve fitting procedure in Excel can be used. It gives

$$JRC_{m_post} = \left[-0.217\ \ln\left(\frac{\Delta u}{\Delta u_p}\right) + 1\right]\ JRC_p \tag{27}$$

The constants $m = -0.217$ and $n = 1$ are fixed values and do not depend on the joint parameters (e.g. JRC, JCS and ϕ_r).

By substituting JRC_{m_pre} from Eq. (26) and JRC_{m_post} from Eq. (27) into the equivalent peak parameters c_t, ϕ_t and ψ_t in Eqs. (15), (16) and (18), respectively, the desired mobilized equivalent M–C parameters c_m, ϕ_m and ψ_m can be obtained for the pre- and post-peak regions. Consequently, the mobilization and degradation of the asperities, signifying the strain hardening and strain softening shear behaviors of rock joints, can now be represented in terms of the M–C parameters. When these mobilized parameters are implemented in a constitutive model for rock joints that uses constant M–C parameters, such as the ubiquitous joint model in the computer code FLAC developed by Itasca (2011), they can enhance the capability of the linear M–C model to portray the nonlinear shear behavior of rock joints. This implementation also suggests that the yield criterion of the linearized B–B model will be in the form of the M–C failure criterion but with the nonlinear characteristic of the B–B criterion.

3.3. Deriving the joint shear stiffness

To develop a constitutive relationship between the shear stress τ and shear displacement Δu, it is also necessary to derive the shear stiffness K_s in the regions of the pre- and post-peak shear displacements. After replacing JRC in Eq. (1) with JRC_{m_pre} and JRC_{m_post} for the pre- and post-peak regions, respectively, K_s in both regions can be obtained by taking the derivative of the resulting τ_m with respect to Δu, i.e. $K_s = \partial\tau_m/\partial(\Delta u)$. Having worked on the derivation, the pre-peak shear stiffness for the region of $\Delta u \le \Delta u_p$ can be obtained as

$$K_{s_pre} = \log_{10}\left(\frac{JCS}{\sigma_n}\right)\ \frac{\pi}{180}\ \sigma_n\ \sec^2\left[JRC_{m_pre}\ \log_{10}\left(\frac{JCS}{\sigma_n}\right) + \phi_r\right] \cdot \frac{a\Delta u_p}{(b\ \ \Delta u + \Delta u_p)^2}\ JRC_p \tag{28}$$

while the post-peak shear stiffness for the region of $\Delta u > \Delta u_p$ can also be obtained as

$$K_{s_post} = \log_{10}\left(\frac{JCS}{\sigma_n}\right)\ \frac{\pi}{180}\ \sigma_n\ \sec^2\left[JRC_{m_post}\ \log_{10}\left(\frac{JCS}{\sigma_n}\right) + \phi_r\right] \cdot \frac{m}{\Delta u}\ JRC_p \tag{29}$$

In summary, the mobilized equivalent parameters c_m, ϕ_m and ψ_m, and the shear stiffnesses K_{s_pre} and K_{s_post} for the pre- and post-peak regions of shear displacement have been derived. These are the parameters for the linearized B–B model that can now be implemented in the linear M–C model so that the nonlinear shear behavior of rock joints can be modeled. The next section will verify the ability of the linearized B–B model to predict joint shear behavior against experimental and numerical results from the literature. The equations presented above are programmed in Excel and used in the validation of the proposed equivalent linear implementation of the B–B model. Research is being conducted to implement the linearized B–B model into the built-in ubiquitous joint model in FLAC (Itasca, 2011).

4. Verifications

Four cases from laboratory and numerical experiments of direct shear tests of rock joints are used to verify the linearized implementation of the B–B model. The standard profiles of joint surface roughness are shown to provide physical visualizations of the corresponding JRC values used in the verifications. These profiles were taken from Barton and Choubey (1977).

4.1. Verifications against experimental results

In this section, the linearized B–B model is verified against the experimental results from Bandis (1980) and Olsson and Barton

(2001), who performed a series of direct shear tests on replicas of rock joints and on natural joints in granite from Äspö in Sweden, respectively. The properties of the joint samples from their experiments are presented in Table 1.

With respect to the experimental results from Bandis (1980), as shown in Fig. 6, the linearized B–B model is able to capture the general trend of shear behaviors of rock joints for all values of joint length and *JRC* with reasonable agreement. When joint roughness decreases, less shear strength is obtained (Fig. 6a) because the joint becomes less dilated (Fig. 6b), indicated by the decrease in the peak dilation angle as shown by the curves of ψ_m vs. Δu (Fig. 6c). The linearized B–B model is also able to capture the effect of roughness reduction on the shear stress after the peak shear strength is reached. This strain softening behavior is more pronounced when the joint is relatively rough with $JRC = 13.6$ than that when the joint is relatively smooth with $JRC = 10.4$, which is consistent with the experimental results (Fig. 6a). The effect of size of the joint sample is also captured. With the decrease in joint length *L*, the shear displacement corresponding to the peak shear stress is observed to decrease, steepening the pre-peak shear stiffness curve. This behavior is also consistent with the experimental results reported by other researchers (Barton and Choubey, 1977; Bandis et al., 1981).

Table 1
Properties of the joint samples used in the laboratory experiments by Bandis (1980) and Olsson and Barton (2001).

Research	*L* (cm)	*JRC*	*JCS* (MPa)	σ_n (MPa)	ϕ_r (°)
Bandis (1980)	18, 12, 6	11.8, 13.6, 16.8	2	0.015	32
Olsson and Barton (2001)	20	9.7	169	2	31

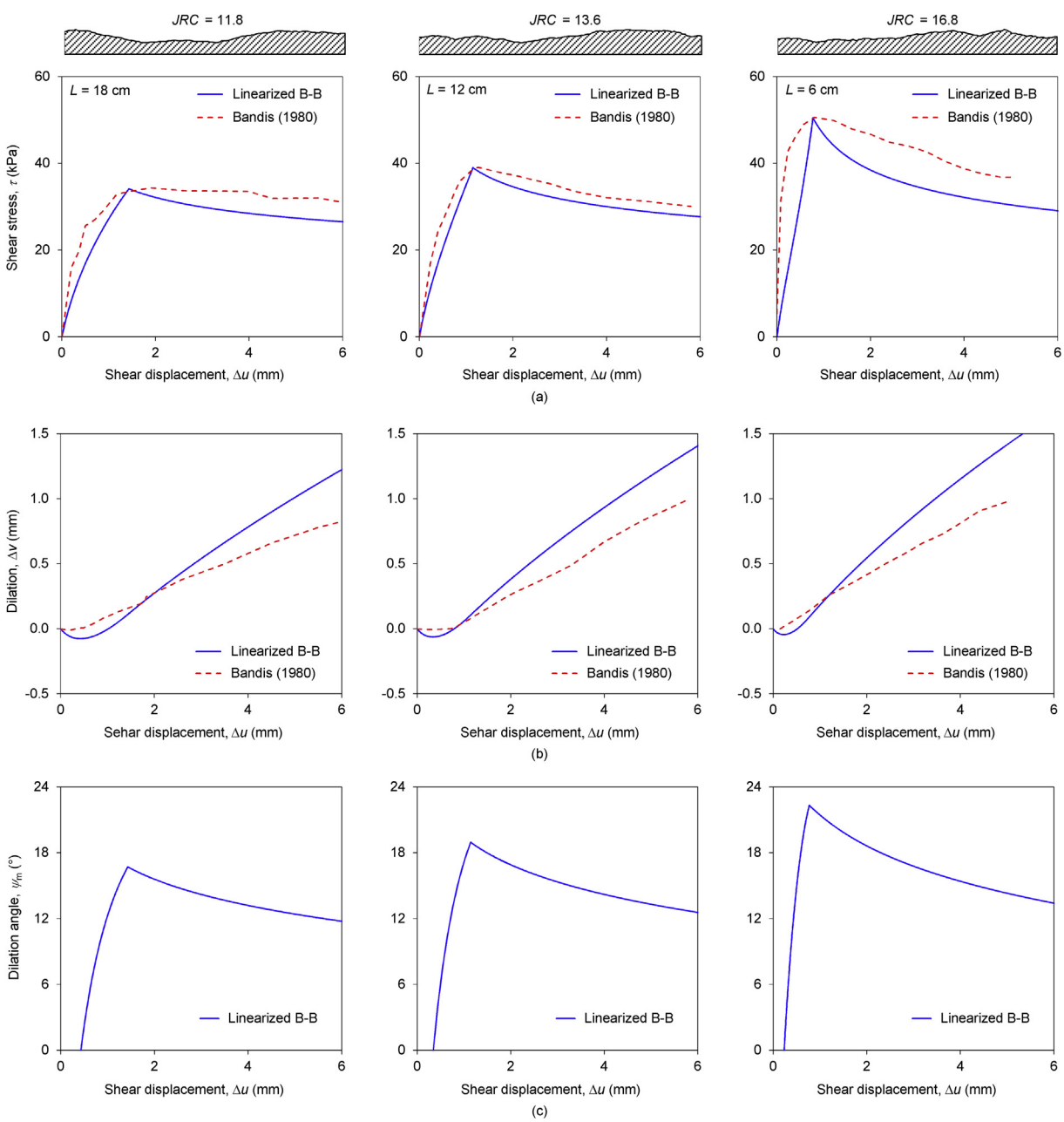

Fig. 6. Comparisons of (a) shear stress and (b) dilation vs. shear displacement from the equivalent linear implementation of the B–B model against experimental results from Bandis (1980), accompanied by (c) curves of dilation angle vs. shear displacement from the linearized B–B model.

Variations of the mobilized cohesion and friction angle with shear displacement for the corresponding joint samples are shown in Fig. 7. The cohesion and friction angle hardening and softening behaviors in the pre- and post-peak regions, respectively, are captured by the linearized B–B model, as well as the increase in the peak values with the increase in *JRC*. As expected, the two parameters increase to their maximum values and then decrease in the softening part, in which a large amount of reduction in the mobilized cohesion is shown. Similar results have been reported by Roosta et al. (2006). It can be noted from Fig. 7 that the cohesion from the linearized B–B model can be smaller than zero—the minimum theoretical limit of joint cohesion—before the dilation starts. Mathematically, the negativity in cohesion is because the origin of the JRC_m/JRC_p curve starts at $-\phi_r/i$, which as defined by Eqs. (13) and (16) will cause c_m to start from a negative value. Physically, this may mean that cohesion still has "zero" influence on the shear strength of rock joints in the early stage of joint shear displacement and that the shear strength of rock joints only depends on the friction angle. Nevertheless, it should be noted that the rate of cohesion change in this early displacement is positive, which is in accordance with the gradual increase in the value of JRC_m/JRC_p.

With respect to the experimental results from Olsson and Barton (2001), the linearized B–B model can reproduce shear stress and dilation curves in good agreement with the test results (Fig. 8). Even though the linearized B–B model slightly overestimates the magnitudes of the peak shear displacement and the shear stress following the failure (Fig. 8a), the model can closely capture the dilation behavior of the joint sample (Fig. 8b).

4.2. Verification against numerical results

The linearized B–B model is also verified against the numerical results from Nguyen and Selvadurai (1998) and Bahaaddini et al. (2013). The former performed shear tests of rock joints in the finite element code FRACON (Selvadurai and Nguyen, 1993; Nguyen and Selvadurai, 1996) considering the asperity damage as a function of plastic work, while the latter conducted tests in the discrete element code PFC2D (Itasca, 2008) using the so-called shear box genesis approach. The properties of the joint samples from the numerical experiments are presented in Table 2. The *JRC* values used by Bahaaddini et al. (2013) are the results from back-calculating the shear strength envelopes presented by Barton and

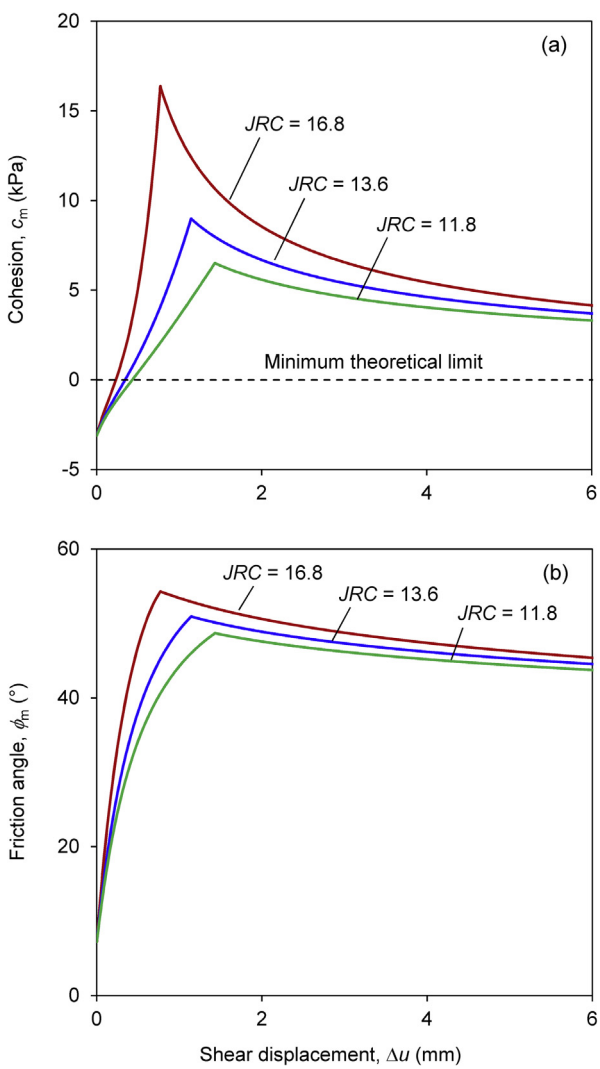

Fig. 7. Plots of mobilized equivalent (a) cohesion and (b) friction angle vs. shear displacement for different *JRC* values for Bandis (1980)'s experiments.

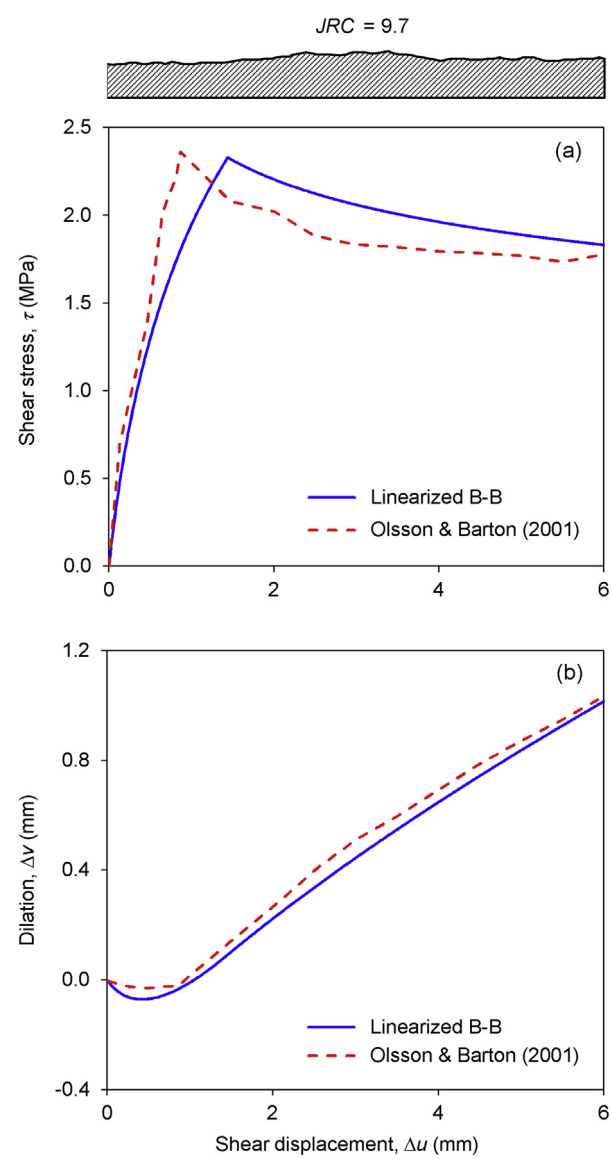

Fig. 8. Comparisons of (a) shear stress and (b) dilation vs. shear displacement from the equivalent linear implementation of the B–B model against the experimental results from Olsson and Barton (2001).

Table 2
Properties of the joint samples used in the numerical experiments by Nguyen and Selvadurai (1998) and Bahaaddini et al. (2013).

Research	L (cm)	JRC	JCS (MPa)	σ_n (MPa)	ϕ_r (°)
Nguyen and Selvadurai (1998)	15	9	28	1, 2, 5	37
Bahaaddini et al. (2013)	10	5.8–18.7	27.4	0.5, 1–5	37.6

Choubey (1977). Out of 10 JRC values used in the numerical experiments by Bahaaddini et al. (2013), only eight of them are verified in this section.

Fig. 9 shows the comparison between the shear behavior from the linearized B–B model and from Nguyen and Selvadurai (1998). A close fit between the shear stress vs. shear displacement curves in both the linearized B–B model and Nguyen and Selvadurai (1998)'s model is observed (Fig. 9a). The shear strength of the joint increases with the increase in the normal stress level, inducing more nonlinear post-peak strain softening behavior. This observation indicates that joints become more brittle at higher normal stress due to the asperities damage that weakens the joint, which is consistent with its shear strength behavior explained in Section 1 (see the explanation for Fig. 2).

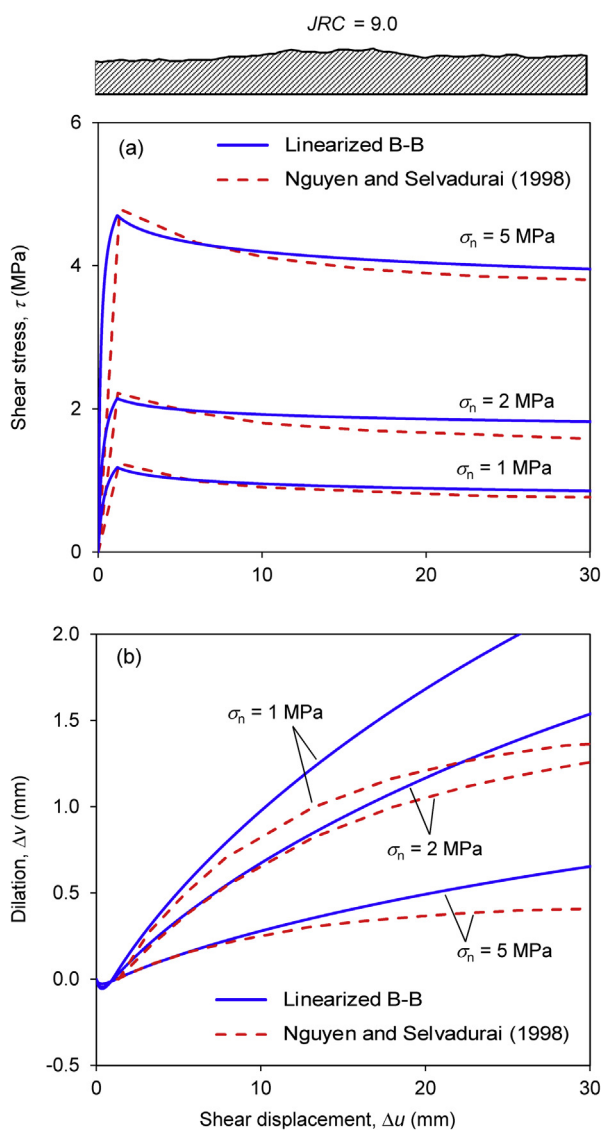

Fig. 9. Comparisons of (a) shear stress and (b) dilation vs. shear displacement from the linearized implementation of the B–B model against the numerical results from Nguyen and Selvadurai (1998).

The comparison for the dilation-induced shear displacement is shown in Fig. 9b. Good agreement is obtained between the linearized B–B model and the numerical experiments within a certain extent of shear displacement, approximately within the range of $\Delta u \leq 10$ mm. For $\Delta u > 10$ mm, the dilation curves from the linearized B–B model are overestimated compared to the numerical experiments.

Overestimation of the dilation behavior has also been seen earlier in Fig. 6b, which shows the comparison of the linearized B–B model against the experimental results from Bandis (1980). While it can be seen from Figs. 6b and 9b that the linearized B–B model may not be able to capture the dilation behavior in great detail, it can certainly capture the general trend of the behavior. Previous results have shown that the linearized B–B model is evidently able to mimic the decrease in the dilation magnitude with the increase in the normal stress and with the decrease in the joint surface roughness. A similar trend is also noticeable for the behavior of peak dilation angle as previously seen in Fig. 6c. Moreover, the linearized B–B model accurately matches the dilation curve from the experimental result given by Olsson and Barton (2001) as seen in Fig. 8b. Furthermore, in all the dilation plots in Figs. 6b, 8b and 9b, the linearized B–B model noticeably captures the contraction behavior at the early stage of shear displacement. Therefore, as included in the linearized B–B model, mobilization of joint surface roughness during shearing is still believed to be the main contribution of the corresponding dilation behaviors of rock joints. While further verifications may be necessary to establish the full capability of the linearized B–B model, this paper provides evidence that the model can predict the general trend of joint shear behaviors and may offer a new insight into the constitutive modeling of rock joints.

Fig. 10 shows the comparison of shear strength envelopes obtained from the linearized B–B model and Bahaaddini et al. (2013) for eight JRC values. The shear strength envelopes from the linearized B–B model match very well with those from the numerical results at various JRC and normal stress values. The nonlinearity in the strength envelopes is well captured by the linearized B–B model and is more pronounced for rough joints ($JRC > 10$) than for relatively planar joint ($JRC < 10$). Similarly, the trend for the peak dilation angle curves obtained from the linearized B–B model are also in good agreement with those from the numerical results (Fig. 11). These results show that the linearized B–B model can reproduce the realistic peak shear strength and peak dilation angle of real joint profiles.

5. Conclusions

A linearized B–B model for predicting the shear behaviors of rock joints was established by directly linking the linear M–C model with the nonlinear B–B model using a tangential technique. This linearization produced the equivalent peak parameters that were expressed in terms of the M–C parameters but consisted of the joint parameters from the B–B model at the same time. These equivalent peak parameters, namely the equivalent peak cohesion c_t, friction angle ϕ_t and dilation angle ψ_t, were further related to joint roughness mobilization and reduction, converting the peak parameters from their constant forms to the mobilized forms, namely the mobilized equivalent cohesion c_m, dilation angle ψ_m and friction angle ϕ_m.

The conversion was done by relating the equivalent peak parameters to the previously constituted discrete-paired values of JRC_m/JRC_p vs. $\Delta u/\Delta u_p$ from the B–B joint model. These discrete points were smoothed out using the proposed continuous

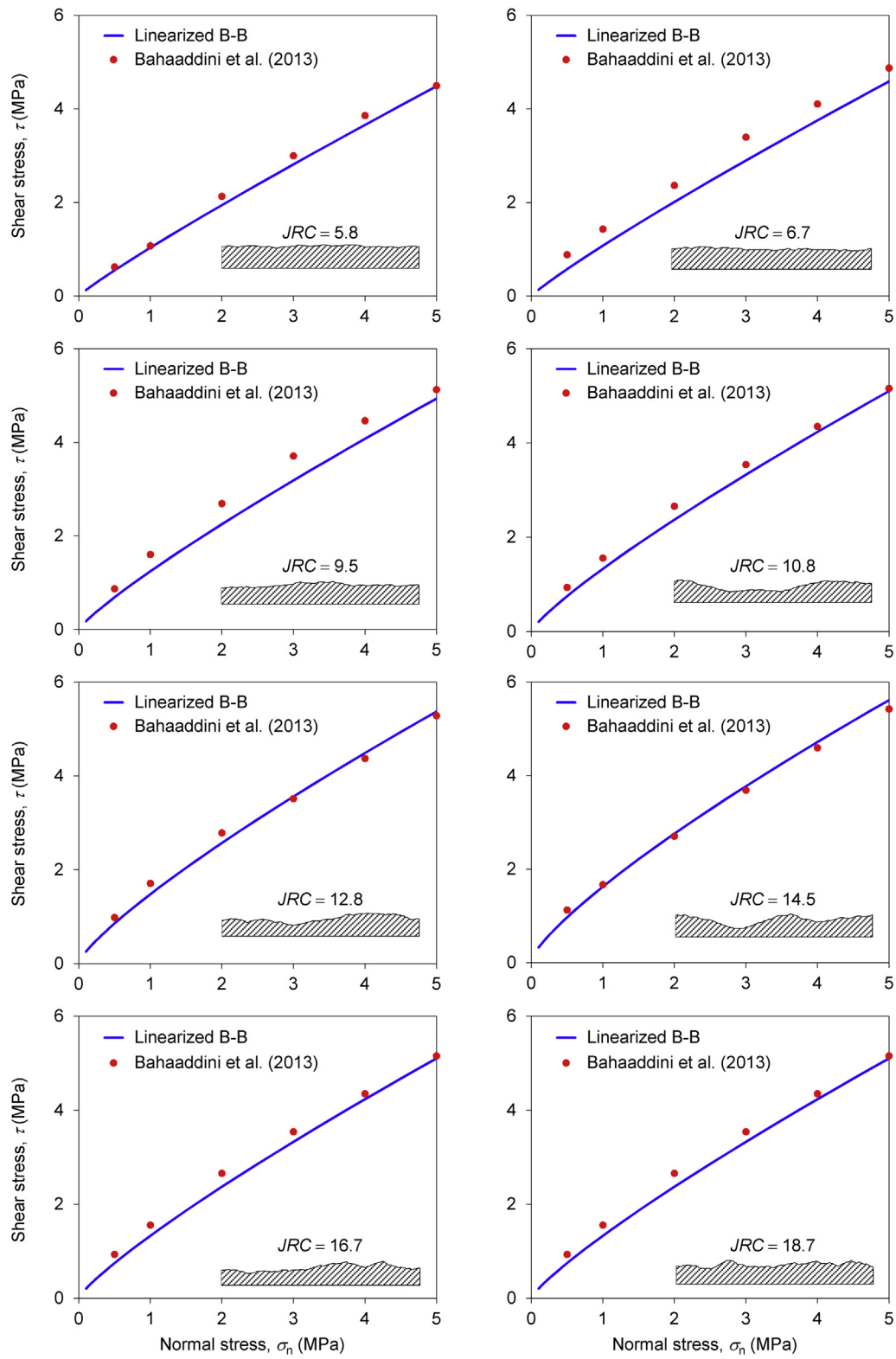

Fig. 10. Comparison of the shear strength envelopes from the linearized implementation of the B–B model against the numerical results from Bahaaddini et al. (2013).

hyperbolic and logarithmic functions to obtain the mobilized joint roughness JRC_m that would govern the shear behaviors in the pre-peak strain hardening and post-peak strain softening regions, respectively. After substituting the resulting JRC_{m_pre} and JRC_{m_post} into the equation for τ and taking the derivative of the resulting τ_m with respect to Δu, the pre- and post-peak joint shear stiffnesses, K_{s_pre} and K_{s_post}, were derived. By doing this, a complete nonlinear shear stress-shear displacement relationship for rock joints was established and represented in terms of the equivalent M–C parameters.

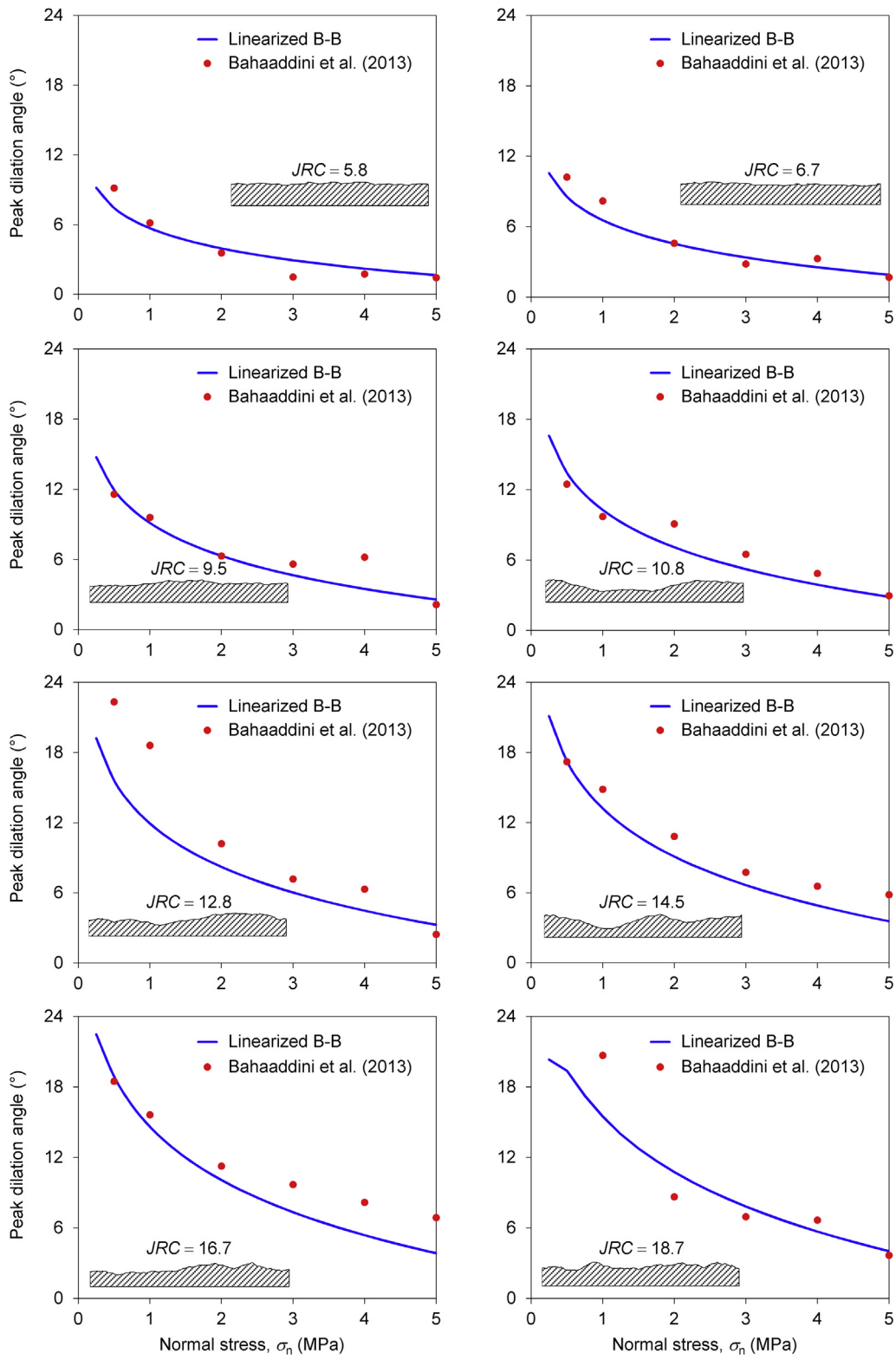

Fig. 11. Comparison of the peak dilation angle curves from the linearized implementation of the B–B model against the numerical results from Bahaaddini et al. (2013).

Verifications against the results from the experimental and numerical direct shear tests showed that the linearized B–B model reproduced realistic shear stress-displacement and dilation-induced shear displacement behaviors under various joint lengths, normal stresses and *JRC* values. The pre-peak strain hardening and the post-peak strain softening behaviors, induced by the mobilization and degradation of joint roughness under shearing, were well represented. The model captured not only the contraction behavior at the early stage of shear displacement but also the dilation behavior at the continuing stage of the displacement. The effect of decreasing joint length on reducing the amount of peak shear displacement and steepening the pre-peak shear stiffness

was properly represented and was consistent with the results reported in other literature. In addition, the nonlinearity of the shear strength envelopes at various *JRC* and normal stress values was also closely reproduced. The nonlinearity was more pronounced for rough joints than that for planar ones, which was consistent with the numerical results.

While further verifications may be necessary, this paper provides evidence that the derivations of the mobilized equivalent parameters and the pre- and post-peak shear stiffnesses in the linearized B–B model are valid, serving their purpose to portray the nonlinear shear behaviors of rock joints. In the future, the linearized B–B model can be potentially applied to computer codes for fractured rock modeling that use the M–C based strain-hardening/softening constitutive model for rock joints. Therefore, neither the benefit of the simplicity of the linear M–C model nor the advanced capability of the nonlinear B–B model is lost.

Conflict of interest

The authors wish to confirm that there are no known conflicts of interest associated with this publication and there has been no significant financial support for this work that could have influenced its outcome.

Acknowledgments

The authors gratefully acknowledge support from the University Transportation Center for Underground Transportation Infrastructure at the Colorado School of Mines for partially funding this research under Grant No. 69A3551747118 of the Fixing America's Surface Transportation Act (FAST Act) of U.S. DoT FY2016.

References

Bahaaddini M, Sharrock G, Hebblewhite BK. Numerical direct shear tests to model the shear behaviour of rock joints. Computers and Geotechnics 2013;51:101–15.
Bandis S. Experimental studies of scale effects on shear strength and deformation of rock joints, 141–54. London: University of Leeds; 1980. p. 287–95.
Bandis S, Lumsden AC, Barton NR. Experimental studies of scale effects on the shear behaviour of rock joints. International Journal of Rock Mechanics and Mining Sciences & Geomechanics Abstracts 1981;18(1):1–21.
Barton N. Review of a new shear–strength criterion for rock joints. Engineering Geology 1973;7(4):287–332.
Barton N. The shear strength of rock and rock joints. International Journal of Rock Mechanics and Mining Sciences & Geomechanics Abstracts 1976;13(9):255–79.
Barton N. Modelling rock joint behavior from in situ block tests: implications for nuclear waste repository design. Report No. ONWI-308. Columbus, USA: Office of Nuclear Waste Isolation; 1982.
Barton N. Non-linear shear strength descriptions are still needed in petroleum geomechanics, despite 50 years of linearity. In: Proceedings of the 50th U.S. rock mechanics/geomechanics symposium. Houston, USA: American Rock Mechanics Association (ARMA); 2016. Paper No. ARMA 16–252.
Barton N, Bandis S, Bakhtar K. Strength, deformation and conductivity coupling of rock joints. International Journal of Rock Mechanics and Mining Sciences & Geomechanics Abstracts 1985;22(3):121–40.
Barton N, Choubey V. The shear strength of rock joints in theory and practice. Rock Mechanics 1977;10(1):1–54.
Barton N, Hansteen H. Very large span openings at shallow depth: deformation magnitudes from jointed models and FE analysis. In: Proceedings of rapid excavation and tunneling conference. Atlanta: American Institute of Mining, Metallurgical, and Petroleum Engineers; 1979. p. 1331–53. Society of Mining Engineers.
Bhasin RK, Barton N. A comparison of Barton-Bandis joint constitutive model with the Mohr-Coulomb model using UDEC. In: Lee HK, Yang HS, Chung SK, editors. Environmental and safety concerns in underground construction: proceedings of the 1st Asian rock mechanics symposium. Seoul, Korea: A.A. Balkema; 1997. p. 413–20.
Deb D. Finite element methods: concepts and applications in geomechanics. New Delhi: PHI Learning Private Ltd.; 2012. p. 158–203.
Goodman RE. Methods of geological engineering in discontinuous rock. San Francisco, USA: West Publishing Company; 1976. p. 158–200.
Goodman RE. Introduction to rock mechanics. 2nd ed. New York: John Wiley & Sons Inc.; 1989. p. 163–4.
Hencher SR, Richards LR. Assessing the shear strength of rock discontinuities at laboratory and field scales. Rock Mechanics and Rock Engineering 2015;48(3):883–905.
Indraratna B, Haque A. Shear behavior of rock joints. Rotterdam, Netherlands: A.A. Balkema; 2000. p. 17–51.
Itasca. PFC™–particle flow code (version 4.0) user's guide. Minneapolis, USA: Itasca Consulting Group; 2008.
Itasca. FLAC®–fast Lagrangian analyis of continua (version 7.0) user's guide. Minneapolis, USA: Itasca Consulting Group; 2011.
Ladanyi B, Archambault G. Simulation of shear behaviour of a jointed rock mass. In: Proceedings of the 11th US symposium on rock mechanics: theory and practice. Berkeley, USA: ARMA; 1969. p. 105–25.
Liu Q, Xing W, Li Y. Numerical built-in method for the nonlinear JRC/JCS model in rock joint. The Scientific World Journal 2014. http://dx.doi.org/10.1155/2014/735497.
Maksimovic M. The shear strength components of a rough rock joint. International Journal of Rock Mechanics and Mining Sciences & Geomechanics Abstracts 1996;33(8):769–83.
Nguyen TS, Selvadurai APS. Modelling of the thermal consolidation of fractured porous media. In: Selvadurai APS, editor. Mechanics of poroelastic media. Dordrecht, the Netherlands: Kluwer; 1996. p. 159–80.
Nguyen TS, Selvadurai APS. A model for coupled mechanical and hydraulic behaviour of a rock joint. International Journal for Numerical and Analytical Methods in Geomechanics 1998;22(1):29–48.
Olsson R, Barton N. An improved model for hydromechanical coupling during shearing of rock joints. International Journal of Rock Mechanics and Mining Sciences 2001;38(3):317–29.
Patton FD. Multiple modes of shear failure in rock. In: Proceedings of the 1st congress of the international society for rock mechanics (ISRM). Lisbon, Portugal: ISRM; 1966. p. 509–13.
Plaxis bv. Plaxis – material models manual. Delft, Netherlands: Plaxis bv; 2016.
Priest SD. Discontinuity analysis for rock engineering. London: Chapman & Hall; 1993. p. 340–81.
Roosta RM, Sadaghiani MH, Pak A, Saleh Y. Rock joint modeling using a visco-plastic multilaminate model at constant normal load condition. Geotechnical & Geological Engineering 2006;24:1449–68.
Selvadurai APS, Nguyen TS. Finite element modelling of consolidation of fractured porous media. In: Proceedings of the 46th annual Canadian geotechnical conference. Saskatoon, Canada: Canadian Geotechnical Society; 1993. p. 79–88.
Simulia. Abaqus 6.12–analysis user's manual. Providence, USA: Dassault Systèmes; 2012.
Singhal BBS, Gupta RP. Applied hydrogeology of fractured rocks. Dordrecht, Netherlands: Kluwer Academic Publisher; 2010. p. 13–33.

Dr. Simon Heru Prassetyo is a Post-doctoral Fellow with the University Transportation Center for Underground Transportation Infrastructure at the Colorado School of Mines. Formerly, he was a mining engineering intern at Leighton Mining, rock mechanics intern at Golder Associates, and geomechanics intern at Henderson Mine, Freeport-McMoRan. He received a BEng in Mining Engineering from Institut Teknologi Bandung, Indonesia, and an MSc in Mining Engineering from West Virginia University (WVU). As a Fulbright scholar at WVU, he was awarded the *Mining Engineering Faculty Award* for his master's thesis on the violent failure of coal specimens under different interface frictions and width-to-height ratios. He recently received a PhD in Civil Engineering from Colorado School of Mines with a doctoral dissertation focused on developing a novel and sequential coupling technique for hydro-mechanical analysis of tunneling in saturated ground. The thesis won the *CEE Spring 2017 Best PhD Dissertation Award*. He is also an active reviewer for several journals and conference papers in rock mechanics and geotechnical engineering.

Dr. Marte Gutierrez is currently the James R. Paden Distinguished Professor at the Department of Civil and Environmental Engineering, Colorado School of Mines. Formerly, he was Post-doctoral Fellow, Senior Engineer and Program Leader at the Norwegian Geotechnical Institute, and Associate Professor/Professor at Virginia Tech. He has held visiting professorship and researcher positions in China, Chile, France, Japan, South Korea and the UAE. He is a member of the Editorial Board of five International Journals. He has published more than 230 papers and is responsible for more than US$ 20 million in research funding. He is a recipient of the Geotechnical Research Medal from UK's Institute of Civil Engineers and the Peter A. Cundall Honorable Mention Award. Dr. Gutierrez's main research interests are in Geomechanics, and Energy and Environmental Sustainability.

Dr. Nick Barton obtained a London University BSc in Civil Engineering from King's College in 1966, and a PhD concerning shear strength and rock slope stability from Imperial College in 1971. He worked for two long periods at NGI in Oslo, and for 4 years at TerraTek in Salt Lake City. Since 2000 he has had his own international rock engineering one-man consultancy, Nick Barton & Associates, based in Oslo and São Paulo. He has consulted on several hundred rock engineering projects in a total of 38 countries during 45 years, has 260 publications as first or single author, and has written two books, one on TBM prognosis, the other linking rock quality and seismic attributes of rock masses at all scales. He is currently writing a book with Bandis: *Engineering in jointed and faulted rock* (expected 2018). He has ten international awards including the 6th Müller Lecture of ISRM. He developed the widely used Q-system for classifying rock masses, and for selecting rock tunnel and cavern single-shell support in 1974. He was originator of the rock joint shear strength parameters *JRC* and *JCS* and co-developer of the resulting Barton–Bandis constitutive laws for rock joint coupled H–M modeling in 1982, which was incorporated as a sub-routine in UDEC-BB in 1985. He has also developed the Q_{TBM} prognosis method and Q_{slope} for selecting maintenance-free rock cutting and bench-face angles. His chief areas of consulting activity have been in hydropower tunneling and cavern construction and performance, nuclear waste disposal site characterization, metro tunnels and caverns, and site characterization at high dams. He has given more than forty keynote lectures in international conferences.